ELSEVIER

Physica D 136 (2000) 303–321

PHYSICA D

www.elsevier.com/locate/physd

Arrays of coupled unstable water jets

F. Giorgiutti *, L. Laurent

Commissariat a l'Energie Atomique, DSM/DRECAM/SPEC, Centre d'Etudes de Saclay, F-91191 Gif sur Yvette Cedex, France

Received 2 June 1998; received in revised form 1 June 1999; accepted 23 June 1999
Communicated by Y. Kuramoto

Abstract

We consider the interaction of oscillators with a noninstantaneous coupling ensured by slow traveling waves. Actually, this particular type of coupling is observed in an experimental system which consists of a bidimensional network of vertical water jets in the presence of a water–air interface: jets rotate and their motions are coupled together through surface waves. Depending on the free jet rotation frequency and of the geometry of the array, this system exhibits various collective modes where the jets synchronise themselves to form phase patterns, rendered sometimes complex by the fact that each jet can rotate clockwise or anticlockwise. A model is proposed which explains many features of the experiment. The dynamics of jets is described by amplitude equations with retarded interaction terms. An interesting point is that the dispersion relation of the surface waves renders the interaction term non linear in a subtle way since its effect depends on the frequency of the limit cycle of the array. This model allows one to determine the possible phase patterns and provides a criterion for the selection process.

PACS: 47.20; 68.10; 68.15

1. Introduction

A vertical jet impinging from below on a water–air interface first pushes upwards a little bump so that the water surface tension equilibrates the jet pressure. For a critical value of the jet velocity U_c (which depends on the depth of the jet nozzle), this bump starts rotating while generating spiral waves which propagate at the surface as shown in Fig. 1. The motion frequency range is between 15 and 50 Hz. As discussed in [1], the jet actually constitutes an "excitator" (it undergoes an helical instability) and, associated to the elastic interface which can be assimilated to a resonator, it oscillates at a frequency ω_0 depending on the interface (surface tension, of fluid) and jet properties (velocity). Then, beyond a jet velocity U_f, the bump is broken and the system enters the "fountain regime".

This paper deals with bumps in the rotating regime. The remarkable feature of such a system is that it can be assembled in arrays [2,11]. As shown in [1], each jet is coupled to the other ones through surface waves and thus,

* Corresponding author. Present address: Laboratoire F.A.S.T., bat. 502, Campus Universitaire, 91405 Orsay Cedex, France. Fax: +33-169-158060.
E-mail address: giorg@fast.u-psud.fr (F. Giorgiutti)

0167-2789/00/$ – see front matter
PII: S0167-2789(99)00157-8

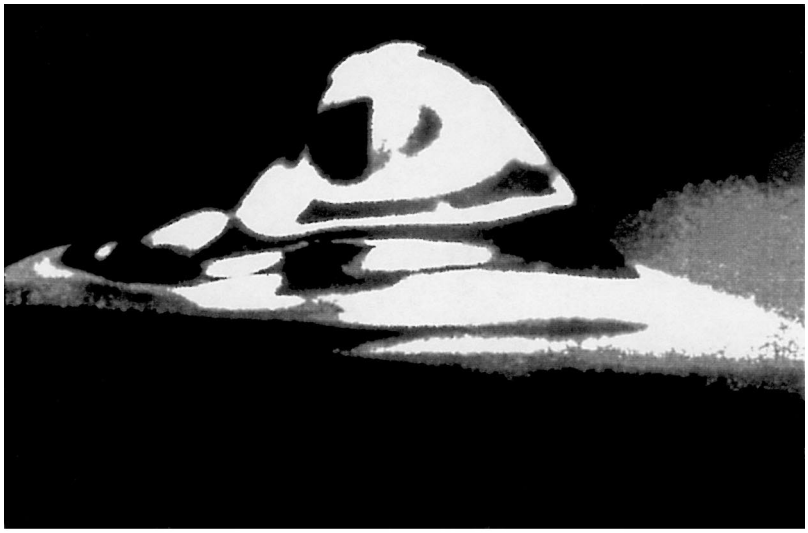

(a)

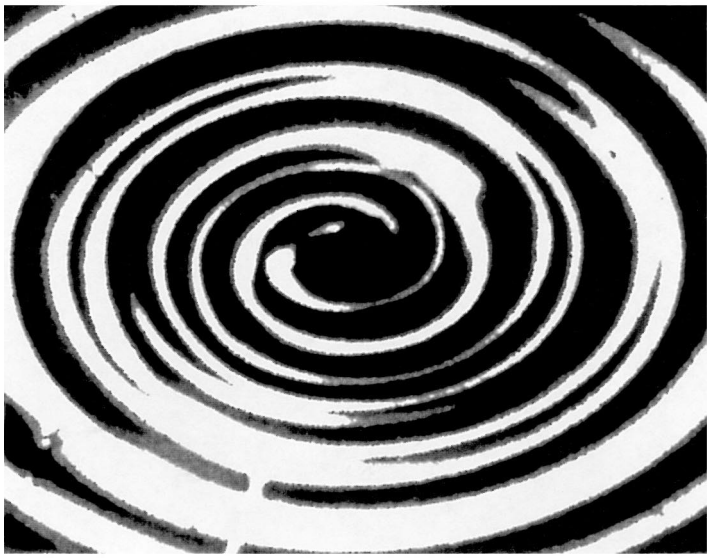

(b)

Fig. 1. Pictures of the bump at the vertical of one jet. (a) The asymmetric rotating bump for $U > U_c$ and (b) the spiral wave generated at the interface by a rotating bump.

through a retarded coupling. Jets can be described as coupled oscillators close to their limit cycle. Such systems have been investigated from a theoretical point of view (see, for instance, [3–6]) and there have been some attempts to achieve experiments based on hydrodynamics which behave as coupled oscillators. This is the case, for instance, of coupled jets [7], wakes [8], boundary layers [9], or vortices [10]. Actually, in experiments with jet arrays, jets synchronize themselves and form various phase patterns with co- or counter-rotating configurations. The jet system described here has some well known properties of "standard" coupled oscillators like synchronisation, and robustness with respect to slight differences between elements. However, jet arrays exhibit three differences with

respect to "standard" coupled oscillators. First the coupling is not instantaneous but ensured by traveling waves propagating at finite velocity while in most of the cases the coupling is either diffusive, i.e. a given jet is sensitive to the information from its neighbours [10] or global when each oscillator is coupled to all the other ones as in many theoretical models. Second, due to the dispersion relation of the waves, the nature of the coupling depends on the frequency of the waves, i.e. of the synchronisation frequency through a phase factor. Finally a rotating jet admits two limit cycles, both signs of ω_0 rendering the collective behaviour richer.

The aim of this paper is to present a model of a coupled oscillator with delayed interaction explaining the experimental results obtained in large arrays. In Section 2, experiments with sets of two jets and periodic triangular or square networks are presented and the main results are summarised. Then, the effect of defects (some jets are lacking) is briefly discussed as on the phase pattern. In Section 3, the model is described. In a first step, the main features of interaction between jets deduced from two jet experiments are recalled. Then the model is extended to large arrays of jets rotating in the same direction. The amplitude equation is solved using an eigenmode analysis valid for infinite networks allowing one to identify possible phase patterns and to discuss the selection mechanisms for the dominant one. Then the model is generalised to situations where the network splits into two counter-rotating subnetworks. In this case no amplitude equation can be found, however a conjecture allowing one to determine the dominant pattern is proposed. In Section 4, experimental results are compared with the predictions of the model. In Section 5, the eigenmode analysis is compared to the result of a direct simulation of coupled oscillators.

2. Experiments

The experimental set up which is similar to the one used in [1,2,11] is presented in Fig. 2. Water enters the injection chamber and gets out through the holes (diameter 1 mm) of the perforated plate. Then the resulting jets impinge from below the water-air interface. The depth of the plates h can be controlled by a micropositioner typically between 5 and 25 mm. The flow velocity U of the jets lie between 0.5–0.7 m/s (the Reynolds numbers are in the range

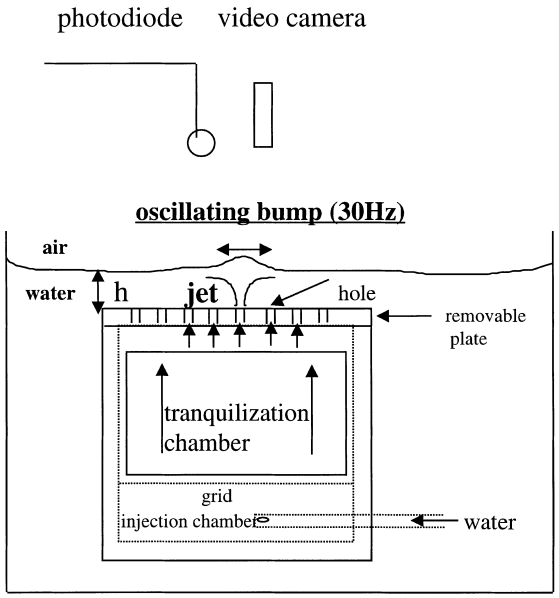

Fig. 2. Experimental setup. h is the depth of the jets under the surface, the holes of the perforated plate are of 1 mm diameter. Only one jet is represented.

250–350). The bump frequencies (15–50 Hz) are measured using a photodiode intercepting the modulated light reflected by the water surface. As shown in [1], the single jet frequency ω_0 varies as $1/U$. Experiments in which the phase pattern in determined as a function of U (i.e. ω_0) are made for various arrays. For this a video camera coupled to a stroboscope is used. For each network a depth is selected and then the velocity of the jet is increased from the critical value U_c to U_f, i.e. the free rotation frequency ω_0 is decreased. Depending on the geometric characteristics of the perforated plate, the depth of the jets and the velocities, various modes are observed. Preliminary experiments have been made with two jet configurations to explain and characterise precisely the nature of the coupling. Then, experiments have been made using square and triangular networks of about 50 jets.

2.1. Observed modes

2.1.1. Two jet configuration

The two jets were separated by distances $6 \times 10^{-3}\,\mathrm{m} < a < 12 \times 10^{-3}\,\mathrm{m}$, the plate being at a constant depth. The coupling between the jets exists for $a < 12 \times 10^{-3}\,\mathrm{m}$. The bumps have always the same direction of rotation and oscillate at the same frequency. When varying the flow rate U or jet spacing, two synchronisation modes are observed: an acoustic mode where the two bumps oscillate in phase and an optical mode where the bumps oscillate in phase opposition. Other effects of the coupling are that the frequency at a given flow rate is different from the free jet one and the critical flow rate, where the bumps start oscillating, is lower for the two coupled bumps than for a single one. The transition between the two modes is accompanied by a phase and frequency jump (see dots in Fig. 5) but this transition is not sudden. Indeed the system hesitates between the two modes in a transition zone. More details can be found in [1].

2.1.2. Square network

We consider now periodic networks. With a square network, defined by the two vectors u and v (see Table 1), at low velocities ($U_c = 0.59\,\mathrm{m/s} < U < 0.61\,\mathrm{m/s}$), a first mode is observed: the optical mode ("diagonal" mode using the terminology of [2,11]) which is represented in Fig. 3(a). All the bumps rotate in the same direction with a frequency between 29 Hz (for 0.61 m/s) and 34 Hz (for 0.59 m/s), and any bump is in phase opposition with its nearest neighbours. If the velocity is increased from 0.61 to $0.65\,\mathrm{m/s} = U_f$, a new mode appears: the "gearing" mode (Fig. 3(b)). Two directions of rotation now coexist, and the network is divided into two sublattices each of them with different directions of rotation. These two sublattices are defined by the two vectors: $(u + v)$ and $(u - v)$, and each of them undergoes an optical mode. The frequency of this mode lies between 22 Hz (for $U = 0.2\,\mathrm{m/s}$) and 20 Hz (for $U = U_f$).

2.1.3. Triangular network

With a triangular network (Table 1), depending on the velocity, two kinds of modes are seen. At low flow rate, $U_c = 0.58\,\mathrm{m/s} < U < 0.63\,\mathrm{m/s}$, a mode with two sublattices and two directions of rotation is identified (Fig. 4(a)). Each sublattice is a rectangular mesh defined by the two vectors $(2u)$ and v. It is in an "optical mode". In this "parallel" mode, the bumps rotate with frequencies between 28 Hz (for $U = 0.62\,\mathrm{m/s}$) and 33 Hz (for

Table 1
Jet arrays used in the experiments

	a	**u** **v**	N	h(depth)	U_c	U_f
Square	12 mm	$a_u(1,0)$ $a_v(0,1)$	57 jets	27 mm	0.59 m/s	0.65 m/s
Triangular	12 mm	$a_u((1/2), \sqrt{3}/2)$ $a_v(1,0)$	48 jets	22 mm	0.58 m/s	0.64 m/s

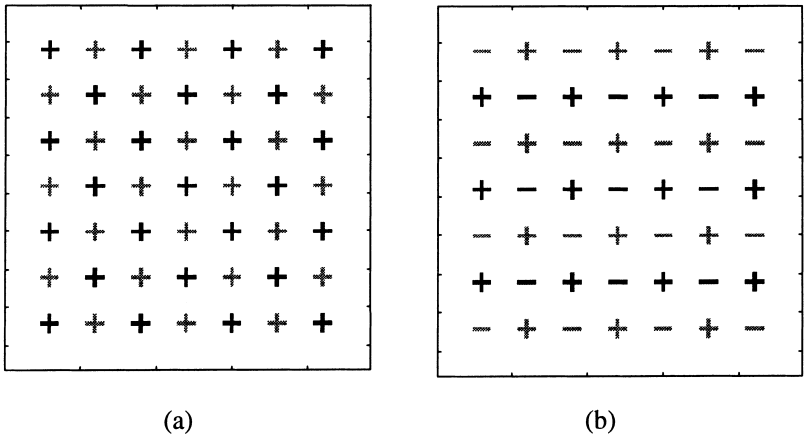

Fig. 3. Various modes observed with a square network: each symbol represents a bump; the symbols "plus" or "minus" define the two different subnetworks; one subnetwork turns clockwise and the other one anticlockwise; in each subnetwork, the different colors mean phase opposition. (a) the optical mode or the optical full network, (b) the gearing mode or the optical subnetwork.

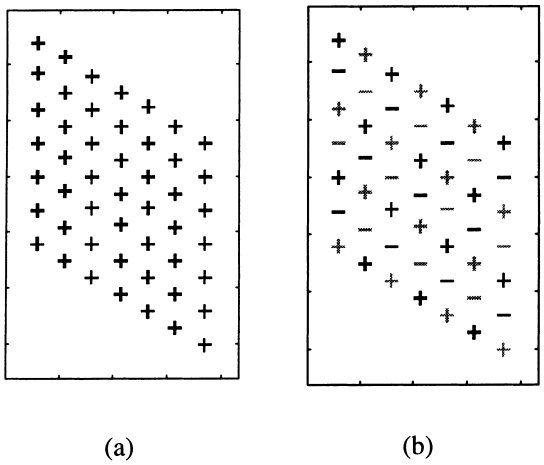

Fig. 4. Various modes observed with a triangular network: (a) the parallel mode and (b) the acoustic mode.

$U = 0.58\,\mathrm{m/s}$). For higher velocities $0.62\,\mathrm{m/s} < U < U_\mathrm{f} = 0.64\,\mathrm{m/s}$, an "acoustic mode" is selected (Fig. 4(b)). All the bumps have the same direction of rotation and are in phase all together. The frequencies of this mode remain bounded in the range 20 Hz (at $U = 0.64\,\mathrm{m/s}$) to 22 Hz (at $U = 0.63\,\mathrm{m/s}$).

2.2. Role of defects in the structure

We have investigated the role of defects in the large networks, by suppressing holes. The results obtained are qualitative because of the nonstationary character of the motion preventing reliable measurements (a faster videocamera or operation with a low surface tension fluid to reduce ω would be required). Whatever the number of blocked holes introduced, the modes corresponding to the upper range of flow rates, acoustic and gearing modes, are robust and are not perturbed by the defects. At low flow rate, where the two subnetworks modes ("optical" or "parallel") appear, consquences are observed, more or less severe depending on the number of defects introduced. For one blocked hole, there is an irresoluteness in the direction of rotation for the nearest bumps of the defect. These particular bumps,

"hesitate" changing their directions of rotation for a few seconds before recovering the "right" one. Concerning the other bumps, the second neighbours of the defect and the others, they are not affected and keep moving as in the absence of defects either in an "optical" mode or in a "parallel" mode. If several defects are introduced, the second or the third neighbours may be affected by the first neighbours. But, nevertheless, considering an average in time and in space, the mode which is recovered is the same as for the configuration with no defect.

3. Modelisation

3.1. Interaction between jets. Case of two-jet systems

When the jet velocity U exceeds the threshold U_c, the bump at the interface is unstable and it starts rotating at frequency ω_0 which is a function of U. In two jet configurations, experiments show that rotation couple at frequency ω slightly different from ω_0. The displacement of jet $m(=1,2)$ with respect to its axis can be expressed as: $x_m + \mathrm{i}y_m = \alpha_m(t)\mathrm{e}^{\mathrm{i}\omega_0 t}$ with $\alpha_m(t) = \alpha\mathrm{e}^{\mathrm{i}(\omega-\omega_0)t+\mathrm{i}\varphi_m}$. Two synchronization modes exist, optical with $\varphi = m\pi$ or acoustic with $\varphi_m = 0$, depending either on jet spacing a or jet velocity U (or ω_0). The dependence on the phase of the coupling and the fact that jets radiate surface waves (see Fig. 1) or can be synchronized by such waves led us to consider a model where the jets were coupled through waves [1]. The simplest equation to describe such a system consists of oscillators close to their limit cycle and coupled by surface waves:

$$\frac{\mathrm{d}\alpha_1}{\mathrm{d}t} - \gamma(1-|\alpha_1|^2)\alpha_1 + \lambda f(a)\alpha_2\mathrm{e}^{-\mathrm{i}k(\omega)a} = 0, \qquad \frac{\mathrm{d}\alpha_2}{\mathrm{d}t} - \gamma(1-|\alpha_2|^2)\alpha_2 + \lambda f(a)\alpha_1\mathrm{e}^{-\mathrm{i}k(\omega)a} = 0. \tag{1a}$$

Or substituting the envelope function by its expression:

$$\begin{aligned} &\mathrm{i}(\omega-\omega_0) - \gamma(1-|\alpha|^2) + \lambda f(a)\mathrm{e}^{-\mathrm{i}k(\omega)a+\mathrm{i}(\varphi_2-\varphi_1)} = 0,\\ &\mathrm{i}(\omega-\omega_0) - \gamma(1-|\alpha|^2) + \lambda f(a)\mathrm{e}^{-\mathrm{i}k(\omega)a+\mathrm{i}(\varphi_1-\varphi_2)} = 0. \end{aligned} \tag{1b}$$

The two first terms in (1a) describe the behaviour of a simple oscillator reaching its limit cycle $|\alpha| = 1$ (the amplitudes are normalized so that the coefficient is 1) and the growth rate is γ. The last term accounts for the coupling through waves. The complex parameter λ is a measure of the strength of the coupling. The wave characteristics are described by an attenuation through the real number $f(a)$ and a phase shift $k(\omega)a$. The wavenumber $k(\omega)$ is obtained from the dispersion equation of the surface wave in deep water taking the actual jet frequency ω : $\omega^2 = gk(1+k^2l_c^2)$ (g is the gravity constant and l_c is the capillary length). It should be noted that the wave propagation may be affected by the radial water flow from the jets. However its average during the propagation between the two jets cancels.

So the behaviour of the jet array is specified by three data: (1) γ (real), the growth rate of the single jet instability, (2) λ (complex), the coupling parameter which governs the interaction between jets and (3) the function $f(a)$ (real).

It is easy to see that the amplitude equation (1b) admits solutions only of $\varphi_1 = \varphi_2 = 0$ or π corresponding to frequencies and amplitudes given by

$$\begin{aligned} &\omega = \omega_0 = \epsilon f(a)|\lambda|\sin(-k(\omega)a + \arg(\lambda)),\\ &|\alpha| = \sqrt{1 - \epsilon\tfrac{|\lambda|}{\gamma} f(a)\cos(-k(\omega)a + \arg(\lambda))} \end{aligned} \tag{2}$$

with $\epsilon = 1$ for $\varphi_1 - \varphi_2 = 0$ or -1 in the other case. It can be shown (see [1]) that only the mode with the largest amplitude is stable and hence should be observed. Comparison with two-jet experiments varying the jet spacing and U allows one to validate this model and to determine $\lambda f(a)$. The argument of λ determines the value of ω_0 at which the transition occurs (when the cosine in Eq. (2) cancels) between two modes, whereas $|\lambda|$ and $f(r)$ determine the value of the frequency jump. This has been done in [1]. The experimental data allow one to fit the argument of λ

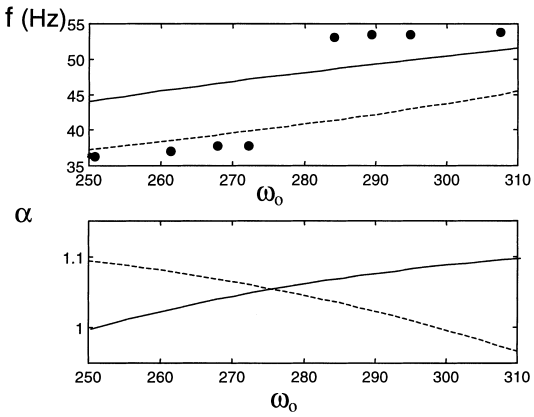

Fig. 5. For two jets with $a = 8.5 \times 10^{-3}$ m, a comparison between the experimental results (dots) and the model (dotted line for the acoustical mode and full line for the optical mode) with the numerical values chosen: $\lambda = 23\mathrm{e}^{-7\mathrm{i}\pi/8}$ and $f(a) = 1$.

to $7\pi/8 \pm \pi/8$ while there was some freedom in the choice of $|\lambda| f(a)$. The experimental results are fitted when this product is in the range 25–30, however the function $f(a)$ could not be determined. Changes in the value of γ had only little importance. An example of comparison of predictions of Eq. (2) with experiment is shown in Fig. 5. The functions $\omega(\omega_0)$ and $\alpha(\omega_0)$ for the two modes defined by Eq. (2) with $a = 8.5 \times 10^{-3}$ m, are plotted. Both the nature of the mode and its frequency correspond to the theoretical prediction.

3.2. Extension of the model to larger networks

One considers now a periodic network of corotating jets which can be generated from a single point with translations along two vectors **u** and **v** of norm a_u and a_v. Any jet $m (m = 1, 2, \ldots, \infty)$ will be defined by two co-ordinates X_m and Y_m (X_m and Y_m are integers). Its displacement with respect to the jet axis as a function of time is given by $x_m + \mathrm{i}y_m = \alpha_m(t)\mathrm{e}^{\mathrm{i}\omega_0 t}$ where $\alpha_m(t)$ is a slowly time varying amplitude.

The two jet model can be generalized to such a network. The simplest equation to describe oscillators coupled by surface waves is

$$\frac{\mathrm{d}\alpha_m}{\mathrm{d}t} - \gamma(U)(1 - \alpha_m\alpha_m^*)\alpha_m + \lambda(U) \sum_{m,n\neq m} \int_{-\infty}^{t} \chi(r_{mn}, t - t')\alpha_n(t')\,\mathrm{d}t' = 0. \tag{3}$$

The integral operator χ represents the effect (retardation and attenuation) of the propagation of the surface wave which is a function of $t - t'$ and of the distance r_{mn} between jets. Actually, since $\alpha_n(t)$ is a slowly varying function, the motion occurs at almost constant frequency (i.e. the frequency does not vary significantly during the propagation time of surface waves between coupled jets). Thus, the integral operator can be simplified so that the effect of the wave propagation from jets n to m is just an attenuation $f(r_{mn})$ and a phase shift $k(\omega_n)r_{mn}$ where $k(\omega_n)$ is the wavevector and r_{mn} the distance between jets n and m. We obtain then the following equation:

$$\frac{\mathrm{d}\alpha_m}{\mathrm{d}t} - \gamma(1 - \alpha_m\alpha_m^*)\alpha_m + \lambda \sum_{n,n\neq m} f(r_{mn})\mathrm{e}^{-\mathrm{i}k(\omega_n)r_{mn}}\alpha_n = 0. \tag{4}$$

The frequency ω_n of jet n is the frequency of $\alpha_n(t)\mathrm{e}^{\mathrm{i}\omega_0 t}$, i.e. ω_0 plus, as a correction, the frequency of $\alpha_n(t)$ averaged over a time Δt (typically the propagation time between coupled jets). The wavevector is given by the dispersion relation of surface waves. Note that the wave propagation is modified by the large scale horizontal flow of the water

escaping from the array. Nevertheless, our array is small enough so that this velocity (a few 10^{-2} m/s) remains small compared to the wave phase velocity (a few 10^{-1} m/s). Note that although the correction $\omega_n - \omega_0$ can be small, the effect of $k(\omega_n)r_{mn}$ is of the order of several wavelengths. For practical applications $f(r_{mn})$ will be taken as a series of coefficients: μ_1 for first neighbours , ... , μ_s for the sth neighbour. By adjusting $\lambda(U)$ it is always possible to normalize μ_1 to one. As will be seen later, the shortest series fitting our results consists in the first three terms. So the behaviour of the jet array is specified by γ, λ, and $f(r)$ as in the two-jet case.

The free jet rotation rate ω_0, which plays a key role in (4) through $k(\omega_n)$ in the coupling term, varies depending on the velocity of the water jet. In fact ω_0 is considered in the following as a control parameter since it can be easily tuned during experiments.

The limit cycles of such a system can be investigated analytically in the limit of infinite arrays so that the symetry of translation can be used. Since all jets lock at the same frequency $\omega_n = \omega$, the appropriate complex amplitudes are of the form $\alpha_m(t) = \alpha e^{i((\omega-\omega_0)t+\varphi_{mo})}$, where α is a real constant. The characteristics of this limit cycle can be found expressing the fact that ω, α and ϕ_m should be such that Eq. (4) is fulfilled:

$$\text{For any } m, \quad i(\omega-\omega_0)\alpha_m - \gamma(1-\alpha^2)\alpha_m + \lambda \sum_{n,n\neq m} f(r_{mn}) e^{-ik(\omega)r_{mn}}\alpha_n = 0. \tag{5}$$

Eq. (5) is equivalent to the search of eigenvectors of operator C defined by

$$\{\psi_m\} \to C\{\psi_m\} = \lambda \left\{ \sum_{n,n\neq m} f(r_{mn}) e^{-ik(\omega)r_{mn}} \Psi_n \right\}, \tag{6}$$

where $\{\Psi_m\}$ is a collection of complex numbers indexed by the jet number. It is convenient to look for solutions periodic in space, with a arbitrary long periods L_u and L_v. Let us introduce the functions

$$F_{pq}(m) = e^{2ip\pi X_m(a_u/L_u)} e^{2iq\pi Y_m(a_v/L_v)} \text{ and } p, q = 0, \pm1, \pm2, \dots, \pm L_u/2a_u.$$

It is easy to check that $\{F_{pq}(m)\}$ are eigenvectors of C.

$$\sum_{n,n\neq m} f(r_{mn}) e^{-ik(\omega)r_{mn}} F_{pq}(n) = \Lambda_{pq} F_{pq}(m) \text{ with } \Lambda_{pq} = \sum_{n,n\neq m} f(r_{mn}) e^{-ik(\omega)r_{mn}} F_{pq}(n) F_{-p-q}(m). \tag{7}$$

This is due to the invariance by translation of the system, so that the sum in (7) does not depend on the choice of m. In the following the jet m will be taken at the origin. Thus $\alpha_m = \alpha e^{i(\omega-\omega_0)t} F_{pq}(m)$ is a solution of Eq. (5) provided α and ω fulfill the condition:

$$\lambda \Lambda_{pq}(\alpha, \omega) + i(\omega - \omega_0) - \gamma(1-\alpha^2) = 0. \tag{8a}$$

The imaginary part of (8a) provides an equation for ω which is a generalisation of Eq. (2):

$$Z_{pq}(\omega) = \omega - \omega_0 + \text{Im}\left[\lambda \sum_{n\neq 0} f(r_n) e^{-ik(\omega)r_n} e^{i(2p\pi a_u X_n/L_u)} e^{i(2q\pi a_v Y_n/L_v)} \right]. \tag{8b}$$

Then the amplitude is given by the real part:

$$\alpha_{pq}^2 = 1 - \frac{1}{\gamma}\text{Real}\left[\lambda \sum_{n\neq 0} f(r_n) e^{-ik(\omega)r_n} e^{i(2p\pi a_u X_n/L_u)} e^{i(2q\pi a_v Y_n/L_v)} \right]. \tag{8c}$$

For a given set (p, q) the function $Z_{pq}(\omega)$ defined by Eq. (8b) has generally one root, but when λ is large enough, often several solutions exist. However solutions too far from ω_0 are not compatible with the use of the amplitude

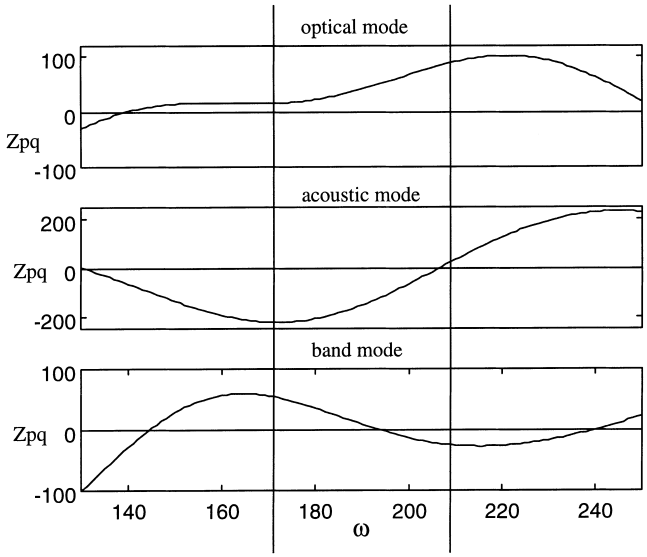

Fig. 6. Function $Z_{pq}(\omega)$ defined by Eq. (8b) for $\omega_0 = 190\,\mathrm{s}^{-1}$. All cases are presented: $p = q = L/2a$ (optical mode), $p = q = 0$ (acoustic mode), $p = 0, q = L/2a$ or $p = L/2a,\ q = 0$ (band mode). The other parameters are $\arg(\lambda) = 7\pi/8$, $\mu_1 = 1$, $\mu_2 = 0.67$, $\mu_3 = 0.2$, and $\gamma = 100$, $a = 12\,\mathrm{mm}$. The vertical bars represent the domain where roots are looked for. In the present case these is a solution for the acoustic mode at $\omega = 206.7\,\mathrm{s}^{-1}$ and for the band mode at $\omega_0 = 193.3\,\mathrm{s}^{-1}$.

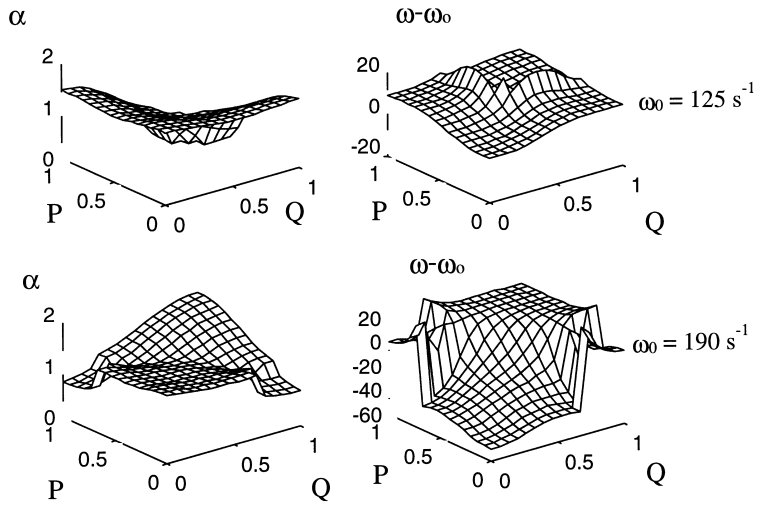

Fig. 7. 3D plots of amplitudes α and frequencies $\omega - \omega_0$ of the modes deduced from Eqs. (8a)–(8c) as a function of ($P = 2ap/L$, $Q = 2aq/L$). The parameters are: $\lambda = 30\exp(-\mathrm{i}7\pi/8)$, $\gamma = 100$, $\mu_1 = 1$, $\mu_2 = 0.5$, $\mu_3 = 0.2$ and the geometry is a square network with $a = 12\,\mathrm{mm}$. The results are displayed for two ω_0 values, top: $\omega_0 = 1255\,\mathrm{s}^{-1}$, bottom: $\omega_0 = 190\,\mathrm{s}^{-1}$.

equation. For this reason only solutions satisfying $(\omega - \omega_0)/\omega_0 < 0.1$ will be considered. An example is shown in Fig. 6. The saturation amplitude of the mode is then given by Eq. (8c) provided the second member of the equation is positive (otherwise the mode has zero amplitude). Eqs. (8a)–(8c) have been solved numerically for various networks so that the amplitudes and the frequency of the modes (p, q) are obtained as a function of ω_0. An example is shown in Fig. 7 which displays the mode amplitudes and frequencies as a function of (p, q) for two values of ω_0 .

All these limit cycles are solutions for the coupled jet motion. However it can be shown (see Appendix A) that only the mode with the largest amplitude should be stable and hence be observed in experiments. It appears that, depending on ω_0, this mode is such that $p = 0$ or $p = L_u/2a_u$ and $q = 0$ or $q = L_v/2a_v$. These modes with the extremum amplitudes correspond to three possible combinations:

1. $p = q = 0$: all the bumps rotate in phase (acoustic mode).
2. $p = L_u/2a_u$, $q = L_v/2a_v$: neighbouring bumps rotate in phase opposition (optical mode).
3. $p = 0$, $q = L_v/2a_v$ or $p = L_u/2a_u$, $q = 0$: jets are in phase in vertical or horizontal bands ("band" mode). There are two band modes (horizontal or vertical wavevector) with the same amplitude.

Note that for a given ω_0, the value of the dominant mode depends also on the relative weights of the interactions between neighbours, i.e. the series μ_s (an example is the difference between Figs. 9 and 10).

3.3. Modes with counter-rotating jets

The results obtained in the previous section are compatible to what is obtained in experiments for 2 or 4 jet sets but slightly different from what is seen on large arrays [2,11]. Indeed, in large arrays, it appears that modes with counter-rotating jets are often preferred. An attempt has been made to explain these features assuming that the coupling term of Eq. (4) had some generality. If the amplitude equation can be generalised to jets rotating in opposite direction, these are to first order not coupled. Indeed the "force" applied on jet m by a counter-rotating jet n is: $F_m(t) = \lambda\alpha_n f(r_{mn})\mathrm{e}^{-\mathrm{i}k(\omega)r_{mn}-\mathrm{i}\omega_0 t-\mathrm{i}\phi_n}$ while the velocity jet m is $V(t) = \mathrm{i}\omega_0\alpha_m\mathrm{e}^{+\mathrm{i}\omega_0 t-\mathrm{i}\phi_n}$. The power exchanged between jets which is proportional to $F_m V^*$ cancels at first order when averaged over one period. The consequences of these properties can easily be seen in a square network by considering the contribution of the eight first neighbours to the motion of a given jet. Taking $\omega = \omega_0$ for the sake of simplicity, Eq. (4) reads:

$$\frac{\mathrm{d}\alpha}{\mathrm{d}t} - \gamma(1 - \alpha\alpha^*) + G(\omega_0, a)\alpha = 0 \tag{9a}$$

with the following conditions:

$$\text{For acoustic mode}: \quad G(\omega_0, a)\alpha = 4\lambda f(a)\mathrm{e}^{-\mathrm{i}k(\omega_0)a} + 4\lambda f(a\sqrt{2})\mathrm{e}^{-\mathrm{i}k(\omega_0)a\sqrt{2}}, \tag{9b}$$

$$\text{for optical mode}: \quad G(\omega_0, a)\alpha = -4\lambda f(a)\mathrm{e}^{-\mathrm{i}k(\omega_0)a} + 4\lambda f(a\sqrt{2})\mathrm{e}^{-\mathrm{i}k(\omega_0)a\sqrt{2}}, \tag{9c}$$

$$\text{for band mode}: \quad G(\omega_0, a)\alpha = 4\lambda f(a\sqrt{2})\mathrm{e}^{-\mathrm{i}k(\omega_0)a\sqrt{2}}. \tag{9d}$$

If the network is split into two subnetworks which ignore each other, one can similarly compute these terms just by considering the four neighbours which are left at a distance $a\sqrt{2}$. For each of these subnetworks the function G can be expressed as follows:

$$\text{For acoustic mode}: \quad G(\omega_0, a)\alpha = 4\lambda f(a\sqrt{2})\mathrm{e}^{-\mathrm{i}k(\omega_0)a\sqrt{2}}, \tag{9e}$$

$$\text{for optical mode}: \quad G(\omega_0, a)\alpha = -4\lambda f(a\sqrt{2})\mathrm{e}^{-\mathrm{i}k(\omega_0)a\sqrt{2}}, \tag{9f}$$

$$\text{for band mode}: \quad G(\omega_0, a)\alpha = 0. \tag{9g}$$

According to Eq. 9(a), the jet interaction is destabilising (acts in the same direction as γ) if the real part of these expressions is negative. Fig. 8 displays for both network and subnetwork geometries the $G(\omega_0, a)$ of the mode with the most real negative value. It appears clearly that below $\omega_0 = 160\,\mathrm{s}^{-1}$ there is only one strongly destabilised mode for subnetwork geometry (counter-rotating jets) while above $170\,\mathrm{s}^{-1}$ the strongest destabilised mode is for a full network or co-rotating jets. There is no simple way of simulating the observed jumps from one system with

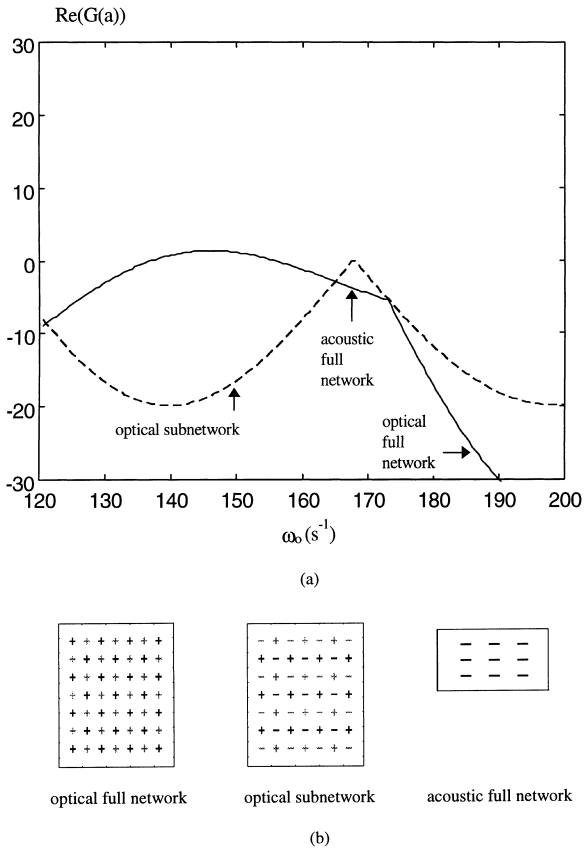

Fig. 8. (a) For both network (plain line) and subnetwork geometries (dotted line) the $\mathrm{Re}(G(\omega_0, a))$ of the mode with the most real negative value as a function of ω_0 for a square network with $a = 12$ mm. The arrows show the mode with the most real negative value. (b) Description of the selected modes.

only co-rotating jets to two counter-rotating networks since ω_0 changes sign (making impossible the use of simple amplitude equations). By extension of this case of co-rotating networks we propose the following conjecture which has to be tested experimentally: *the observed mode is the one with the largest amplitude considering both co-rotating networks and one half of the network.*

4. Comparison with experiments for periodic networks

For the configuration corresponding to experiment the amplitudes of eigenmodes have been computed. For each geometry (square and triangular) full networks and the relevant partitions into two equal subnetworks are considered. The full network is defined by the two vectors u and v which can lead to two modes with co-rotating jets. The subnetworks corresponding to the observations described above are defined by the two vectors $(u + v)$ and $(u - v)$ in the square network and $(2u, v)$ in the triangular geometry. The amplitudes and frequencies of each mode are computed for the full network or a subnetwork and the dominant mode is sorted.

The parameters must be adjusted to simulate the observed mode configuration and the frequency jumps. If one adds an additional constraint to fit the two jet experiments discussed in Section 3.1, λ is determined. By comparing

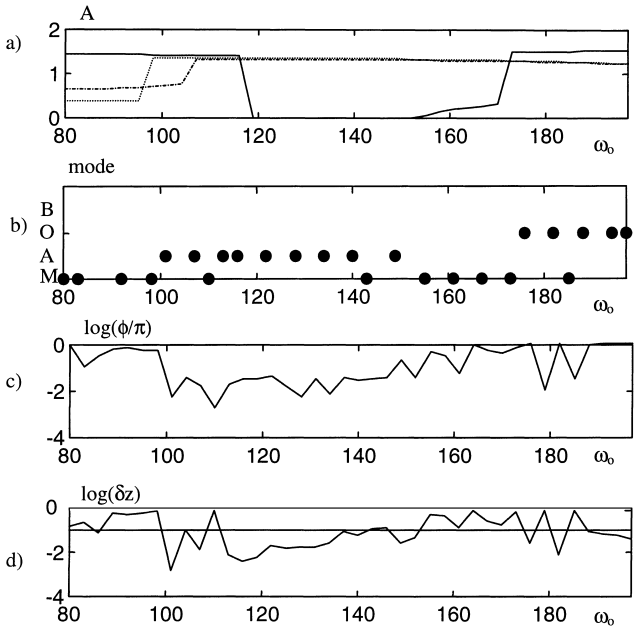

Fig. 9. Comparison of the results of the eigenmode analysis and time evolution code for a square network as a function of ω_0. The parameters are $a = 12\,\text{mm}$, $\lambda = 30\exp(-\text{i}7\pi/8)$, $\gamma = 100$, $\mu_1 = 1$, $\mu_2 = 0.5$, $\mu_3 = 0.2$. (a) Amplitude A of optical mode (full line), acoustic mode (dashed line) and band mode (dash dotted line) predicted by the eigenmode analysis for an infinite network. (b) Phase pattern obtained from the evolution code after 12 s (6×6 network): B=band mode, O=optical mode, A=acoustic mode, M=mixture of modes. (c) Log (Φ/π), where Φ is the relative phase variation between the two last time slices for the time evolution in a 6×6 network. (d) Measure $\log(\delta z)$ of the mode purity as defined in Section 4. If it is larger than -1, the mode is called "mixed".

Figs. 9(a) and 10(a), it can be seen that the weights μ_s govern the mode repartition. Various forms for μ have been tested including a direct dependence on distance. However the best results are obtained when the relevant parameter is the rank of neighbouring network, suggesting that the capillary wave scattering by jets is the dominant loss source rather than the damping of waves. For the μ_s, a parameter scan has been made in the space $\mu_2 - \mu_3$ (note that $|\lambda|$ is normalised so that $\mu_1 = 1$). The results are shown in Fig. 11 for a square network. We can visualize the zone where the dominant eigenmodes correspond to the one seen in all experiments. Figs. 12 and 13 show an example: the chosen parameter set allows us to reproduce both the frequencies and modes observed in the experiment for the square and the triangular networks.

5. Comparison with simulations

5.1. Description of the evolution code

In experiments the system differs from the infinite network discussed above at least for two reasons: First the networks used in experiments have finite size (typically 50 jets) and second there is a spread in the ω_0 values (scatter of a few per cent of the hole diameters). To see how these features may affect the results of the infinite network theory, a time evolution code has been written to describe the behaviour of a finite array of coupled jets following Eq. (4). Note that these equations are valid only in quasi-stationary conditions for co-rotating networks, because the coupling term is only correct when the motion is harmonic so that $k(\omega_n)r_{mn}$ is well defined. Moreover the frequency and hence the coupling terms are not known a priori so that an interative procedure must be used.

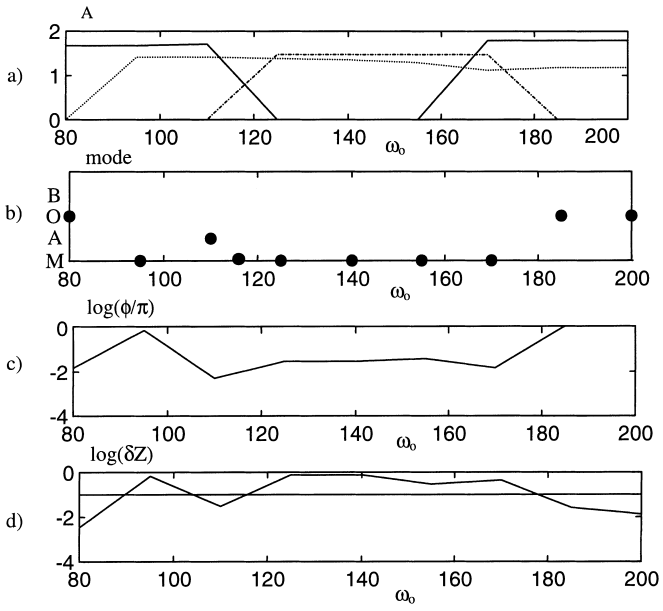

Fig. 10. Comparison of the results of the eigenmode analysis and time evolution code for a square network as a function of ω_0. The parameters are $a = 12\,\text{mm}$, $\lambda = 30\exp(-\text{i}7\pi/8)$, $\gamma = 100$, $\mu_1 = 1$, $\mu_2 = 1$, $\mu_3 = 0$. (a) Amplitude A of the optical mode (full line), acoustic mode (dashed line) and band mode (dash dotted line) predicted by the eigenmode analysis for an infinite network. (b) Phase pattern obtained from the evolution code after 12 s (6×6 network): B=band mode, O=optical mode, A=acoustic mode, M=mixture of modes. (c) $\text{Log}(\Phi/\pi)$ where Φ is the relative phase variation between the two last time slices for the time evolution in a 6×6 network. (d) Measure $\log(\delta z)$ of the mode purity as defined in Section 4. If it is larger than -1, the mode is called "mixed".

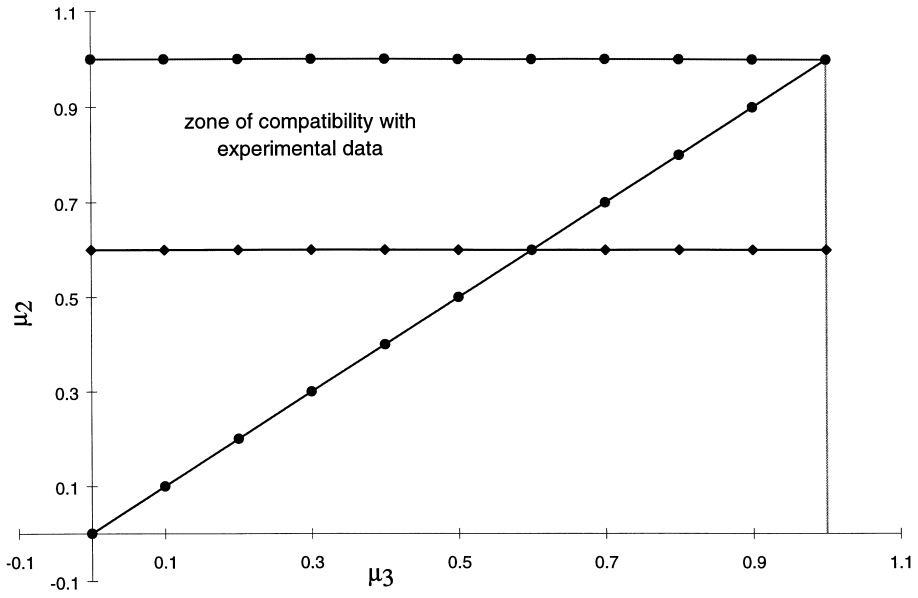

Fig. 11. Domain in the $\mu_2 - \mu_3$ space where results compatible with experimental data are obtained for square networks.

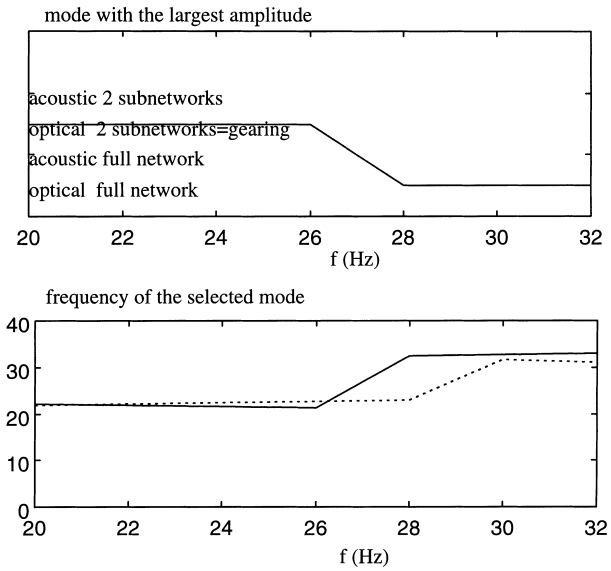

Fig. 12. Phase and frequency obtained by the eigenmode analysis for $\mu_2 = 0.67$, $\mu_3 = 0.2$ for a square network; dotted line = optical subnetwork and full line=optical network.

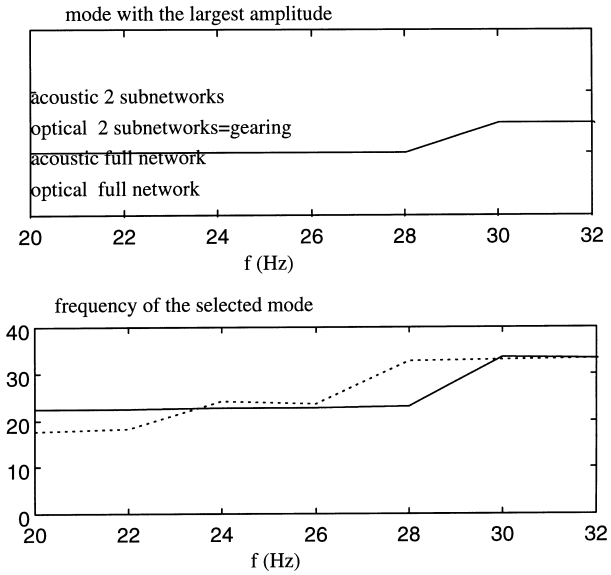

Fig. 13. Phase and frequency obtained by the eigenmode analysis for $\mu_2 = 0.67$, $\mu_3 = 0.2$ for a triangular network; dotted line = optical subnetwork and full line = acoustic network.

1. The amplitudes are initialised with a frequency ω_0 and random phase ϕ_m and amplitude (< 0.05). Then the system is followed during a time of order of $1/\gamma$ until the amplitude reaches a quasi-stationary value.
2. Then the iterative procedure takes place. The system is integrated during a few periods of the rotation motion of the envelope, typically $\Delta T = 100\pi/\omega_0$. A Fourier analysis allows one to get the actual frequencies ω_n which are used to "refresh" the coupling term which is replaced by a weighted average of ω_0 and ω_n for the following time slice.

3. The same procedure is applied to the following time slices till the system converges. The frequencies ω_n are followed as a function of the number of iterations to check that the code converges. An additional convergence criterion is obtained by measuring at any time slice the phase difference between the jet and a reference one. When this phase difference does not depend on time the jets are phase locked. Typically the rquired number of iterations is 10 in standard cases.
4. For any time slice the dominant mode is identified. The quantity $\phi_{kn} = \arg(z_n F_{-k}(n))$ is computed for k corresponding to optical, acoustic, both band modes. The identified mode corresponds to the k value so that the standard deviation of ϕ_{kn} at fixed k is minimum (it is zero for a pure mode). For this identification procedure the edges which may have sometimes "pathological phases" are eliminated.

Simulations are made for various values of ω_0 keeping constant values of γ and λ. The outputs of the code are the curves $\omega(\omega_0)$ and $\phi_{kn}(\omega_0)$ which fit the data. An example is given in Fig. 14 with the trajectories of the α_m for a 6×6 square array ($a = 12\,\mathrm{mm}$) and $\omega_0 = 140\,\mathrm{s}^{-1}$. The function f is given by $\mu_1 = 1$, $\mu_2 = 0.5$ and $\mu_3 = 0.2$ (the ones corresponding to Fig. 9). In the time lag $t = 0$–$0.3\,\mathrm{s}$ the amplitude of the jet grows till the limit cycle is reached (Fig. 14(a)). Then the jets follow this cycle as shown in Fig. 14(b). An acoustic mode can be clearly identified. However the amplitude is jet-dependent, especially at the edge where it has a lower value. Note that at the beginning the code is also adjusting the phases of the coupling coefficients, i.e. $\mathrm{e}^{-\mathrm{i}k(\omega_n)r_{mn}}$ so that the trajectory of the system in Fig. 14(a) is not exactly the actual one while for longer times the system has converged to the stationary state, i.e. which is an actual solution of Eq. (4). The convergence of the code is illustrated in Fig. 14(c) where for five runs (the initial conditions are random) the frequency, the logarithm of phase slip between time slice, $\log(\phi)$ and the identified mode are plotted as a function of the iteration number. Then the code has been used to investigate the two following points.

5.2. *Effect of the scatter in ω_0*

The code has been used to test the rubustness of the rotation modes with respect to a scatter in the values of ω_0. A modified version of Eq. (4) is also considered in which jets have slightly different free rotation frequencies, for instance, to account for a scatter in the diameters. This frequency is a random variable centered around ω_0, i.e. $\omega_0 + \nu(m)$ where $\nu(m)$ is a uniform probability distribution in $[-\delta, +\delta]$. Eq. (4) becomes:

$$\frac{\mathrm{d}\alpha_m}{\mathrm{d}t} + \mathrm{i}\nu_m\alpha_m - \gamma(1 - \alpha_m\alpha_m^*)\alpha_m + \lambda\sum_{m\neq n} f(r_{mn})\mathrm{e}^{-\mathrm{i}k(\omega_n)r_{mn}}\alpha_n = 0.$$

For the series $\mu_1 = 1$, $\mu_2 = 0.5$, $\mu_3 = 0.2$ and $\lambda = 30\,\mathrm{e}^{-7\mathrm{i}\pi/8}$ a scan in δ has been performed for various ω_0. We have represented in Fig. 15, for a square network (5×5), the value of δ for which there is no more synchronisation ($\delta_{\max}$) as a function of ω_0. As this was the case for the two-jet case [1] it appears that the system has some robustness ($\delta_{\max} > 5\,\mathrm{s}^{-1}$) with respect to perturbations except close to the transition frequency, i.e. $\omega_0 \sim 170\,\mathrm{s}^{-1}$ as seen in Fig. 9(a) when the optical mode amplitude crosses that for the acoustic mode.

5.3. *Comparison of the asymptotic regimes predicted by eigenmode analysis and the code*

It is interesting to study the finite size effects by comparing the asymptotic regime predicted by the evolution code for a finite network with expectations from the selection mechanism discused in Appendix A for infinite networks. This has been done for two functions f, first $\mu_1 = 1$, $\mu_2 = 0.5$, $\mu_3 = 0.2$ and second $\mu_1 = 1$, $\mu_2 = 1$, $\mu_3 = 0$. According to the eigenmode analysis the first set of μ_s leads to an acoustic mode for $120\,\mathrm{s}^{-1} < \omega_0 < 165\,\mathrm{s}^{-1}$, optical outside this range. For the second set of μ_s the band modes are the ones with the largest amplitude for

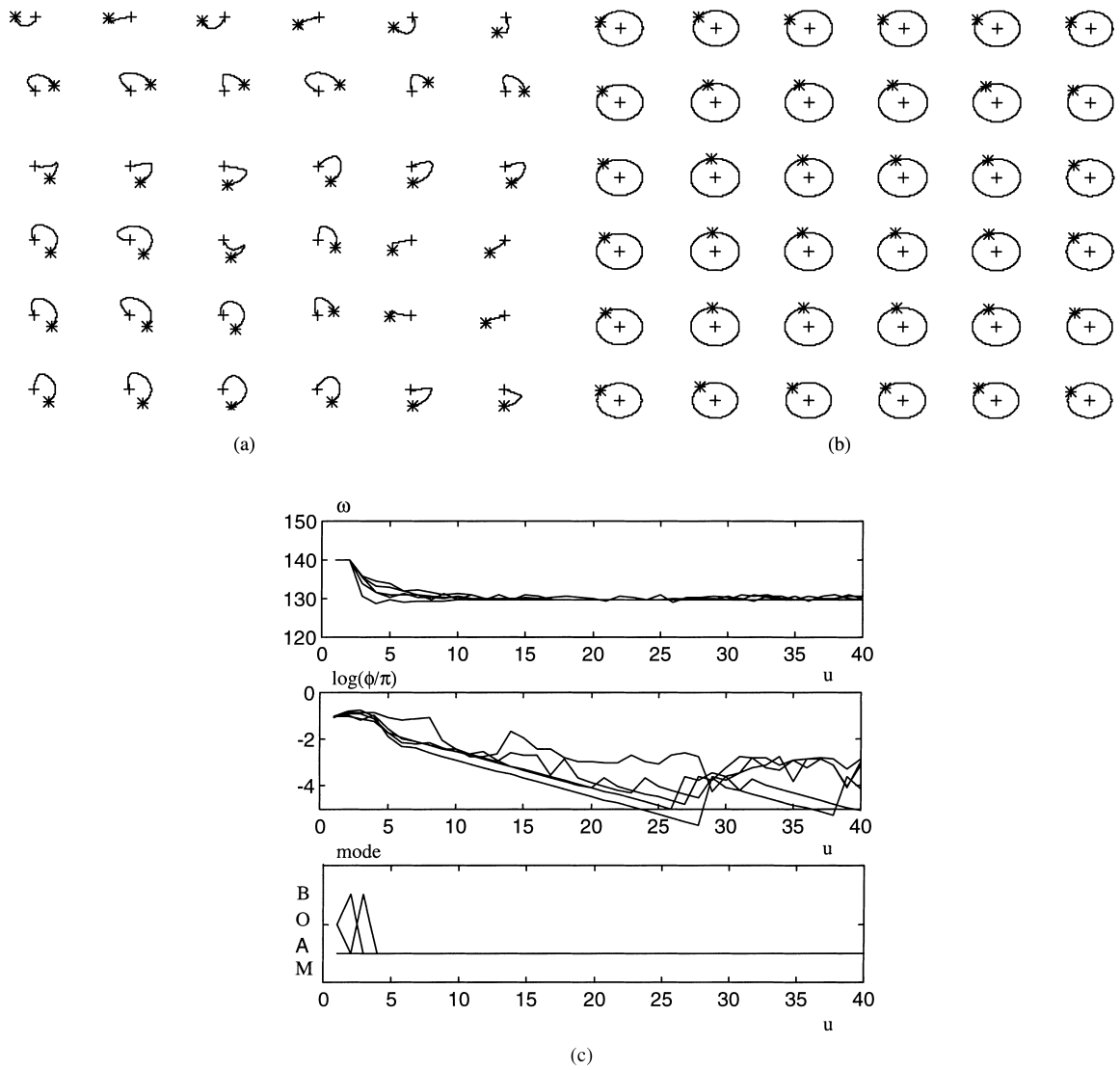

Fig. 14. Square network (6×6, mesh $= 12$ mm), trajectories of the envelopes α_n in the complex plane. The parameters are $\lambda = 30\exp(\mathrm{i}7\pi/8)$, $\mu_1 = 1$, $\mu_2 = 0.5$, $\mu_3 = 0.2$, $\gamma = 100$, $\omega_0 = 140\,\mathrm{s}^{-1}$. (a) Example of start up between $t = 0$ and 0.3 s for $\omega_0 = 140\,\mathrm{s}^{-1}$. The stars represent the position of the bump at the end of the time slice and the cross is the origin. (b) Asymptotic regime $t = 51$–52 s for $\omega_0 = 140\,\mathrm{s}^{-1}$, i.e. when the expected one is the acoustic one (see also Fig. 9). The star represents the position of the bump at the end of the time slice and the cross is the origin. (c) For 5 runs: evolution of frequency ω, of $\log(\Phi/\pi)$, the log of average phase slip between time slices and of the identified mode as a function of the number of iterations u for $\omega_0 = 140\,\mathrm{s}^{-1}$. B=band mode, O=optical mode, A=acoustic mode, M=mixture of modes.

$110\,\mathrm{s}^{-1} < \omega_0 < 170\,\mathrm{s}^{-1}$, while the acoustic mode dominates outside. This mode repartition can be seen in Figs. 9(a) and 10(a). A finite network (6×6) has been evolved for various ω_0 for both series of μ_s. Some results of the time evolution code are displayed in Figs. 9(a) and 10(b). It appears that the evolution code converges to cycles compatible with the prediction of the eigenmode analysis.

- When the dominant mode is either the optical or the acoustic mode, the evolution code converges most of the time of this mode. However the mode is somewhat distorted by the presence of the edge as shown by the standard deviation δz of the ϕ_n which stays often in the range 10^{-3}–10^{-1} (above 10^{-1} the mode is considered to be mixed).

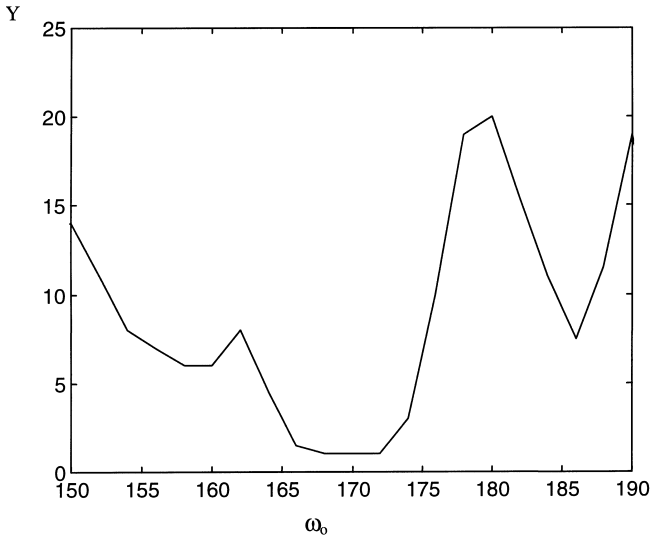

Fig. 15. Value of $Y = \delta_{\max}$ as a function of ω_0 obtained with the time evolution code running. The other parameters are $\mu_1 = 1$, $\mu_2 = 0.5$, $\mu_3 = 0.2$, $\lambda = 30\,\mathrm{e}^{-\mathrm{i}7\pi/8}$ and $\gamma = 100$. The network is a square. 5×5 array with $a = 12\,\mathrm{mm}$.

One can also note that when at large frequencies the dominant mode is the optical one the normalised phase slip ϕ/π between time slices is rather high indicating that the limit cycle remains rather noisy.

- When the dominant mode is the band mode the resulting motion, although coherent (it is phase locked), does not correspond to a well identified mode but is rather a mixture. This is coherent with the fact that the eigenmode analysis predicts no stable dominant mode.

6. Conclusion

This work was motivated by experimental results obtained on water jets which exhibit a wide variety of collective behaviour. This leads us to introduce a new model of coupled, nonlinear and synchronised rotators. It appears that by fitting two parameters (complex coupling strength and attenuation as a function of jet relative positions) this model explains a wide variety of observations involving the frequency of rotation, mode structure, spontaneous splitting into subnetworks, this for various configurations (limited set of jets, large square or triangular networks). Two ingredients are required to explain the observed behaviour of the rotators:

- An amplitude equation in which the jets are coupled together through a retarded interaction term. For infinite networks this equation can be transformed into a linear one and the phase patterns observed in the networks are the eigenmodes of the operator.
- A criterion for the mode selection which is based on consideration of the nonlinear behaviour of the solutions. If one considers only jets rotating in the same direction, it can be shown analytically for infinite networks that only the mode with the largest amplitude is stable. This criterion is extended to configurations including counter-rotating subnetworks.

This new model offers interesting new features. First, due to the fact that the coupling between each element is due to travelling waves, in a dispersive medium there is a subtle interaction between the limit cycle frequency and the coupling which in numerical simulation requires the use of an iterative scheme. Second, each rotator can have positive or negative rotation frequency, i.e. two possible limit cycles are allowed. The system can “select” the repartition of these two limit cycles to optimise the interactions.

Acknowledgements

The authors would like to thank François Daviaud for valuable comments.

Appendix A. Phase pattern selection in an infinite network

Above it has been seen that many modes could be possible limit cycles for an infinite network. It is interesting now to test their stability. Let us assume that the system oscillates around a limit cycle defined by the couple of wavenumbers $(p_0, q_0) = i_0$ corresponding to the frequency ω_{i0} and amplitude α_{i0}. The displacement of jet m is given by $\alpha_m = \epsilon_{i0} e^{i(\omega_{i0}-\omega_0)t} F_{i0}(m)$ where $\epsilon_{i0} = \alpha_{i0}$ and $F_{i0}(m)$ are defined in Section 3.2. A perturbation of the displacement can be expressed as a superposition of contributions of the modes $j = (p_j, q_j)$ i.e. $\delta\alpha_m(t) = \sum_j \epsilon_j(t) e^{i(\omega_j-\omega_0)t} F_j(m)$ where the $\epsilon_j(t)$ are time varying complex amplitudes. The equation of motion of bump m can be linearized and projected on each mode k.

$$\text{The non linear term:} \quad (\alpha_m + \delta\alpha_m)^2(\alpha_m + \delta\alpha_m)^* = \sum_{i,j,h} \epsilon_i \epsilon_j \epsilon_j^* e^{i((\omega_i+\omega_j-\omega_h-\omega_0)t)} F_i(m) F_j(m) F_h^*(m),$$

$$\text{can be linearized into:} \quad \alpha_{i0}^2 \left(\sum_h \epsilon_h^* e^{i((2\omega_{i0}-\omega_h-\omega_0)t_i)} F_{i0}^2(m) F_h^*(m) + 2\epsilon_h e^{i((\omega_h-\omega_0)t)} F_h(m) \right).$$

At this point it is convenient to introduce the mode with the index $k' = (2p_0 - p_k, 2q_0 - q_k)$ so that $F_k(m) = F_{i0}^2(m) F_{k'}^*(m)$, i.e. the mode coupled to the kth through nonlinear effects. Thus the linearized amplitude equation for the Fourier component F_k reads:

$$i(\omega_k - \omega_0)\epsilon_k + \frac{d\epsilon_k}{dt} - \gamma(1 - 2\alpha_{i0}^2)\epsilon_k + \lambda\epsilon_k \sum_{m\neq n} f(r_{mn}) e^{-ik(\omega_k)r_{mn}} F_k(n) F_{-k}(m) = -\gamma\alpha_{i0}^2 \epsilon_{k'}^* e^{i(2\omega_{i0}-\omega_{k'}-\omega_k)t}. \tag{A.1}$$

Note the right-hand side varies in time only because of the nonlinearity of the relation of dispersion of the modes, i.e. slowly with time. Eq. (5) applied to the mode k gives

$$i(\omega_k - \omega_0)\epsilon_k - \gamma(1 - \alpha_k^2)\epsilon_k + \lambda\epsilon_k \sum_{m\neq n} f(r_{mn}) e^{-ik(\omega_k)r_{mn}} F_k(n) F_{-k}(m) = 0, \tag{A.2}$$

where α_k is the saturation level of this model when it is alone. By substracting Eq. (A.2) from (A.1), we obtain an equation for ϵ_k. Similarly an equation can be obtained for $\epsilon_{k'}^*$ by permuting k and k' and taking the conjugate. The resulting equations are:

$$\frac{1}{\gamma}\frac{d\epsilon_k}{dt} = (\alpha_k^2 - 2\alpha_{i0}^2)\epsilon_k - \alpha_{i0}^2 \epsilon_{k'}^* e^{i(2\omega_{i0}-\omega_{k'}-\omega_k)t},$$

$$\frac{1}{\gamma}\frac{d\epsilon_{k'}^*}{dt} = (\alpha_{k'}^2 - 2\alpha_{i0}^2)\epsilon_{k'}^* - 2\alpha_{i0}^2 \epsilon_k e^{i(2\omega_{i0}+\omega_{k'}+\omega_k)t}.$$

This is a linear system with coefficients varying slowly in time. An approximate (time varying) growth rate can be found assuming that these coefficients are frozen. The eigenvalues follow the relation:

$$\lambda(t)^2 - \lambda(t)(\alpha_k^2 + \alpha_{k'}^2 - 4\alpha_{i0}^2) + (\alpha_{k'}^2 - 2\alpha_{i0}^2)(\alpha_k^2 - 2\alpha_{i0}^2) - \alpha_{i0}^4 = 0$$

The stable zone, i.e. when the real parts of the eigenvalues $\lambda(t)$ are negative, can be drawn in the $\alpha_k^2/\alpha_{i0}^2 - \alpha_{k'}^2/\alpha_{i0}^2$ space as shown in Fig. 16. It is interesting to note that when the cycle i_0 corresponds to one of the three modes

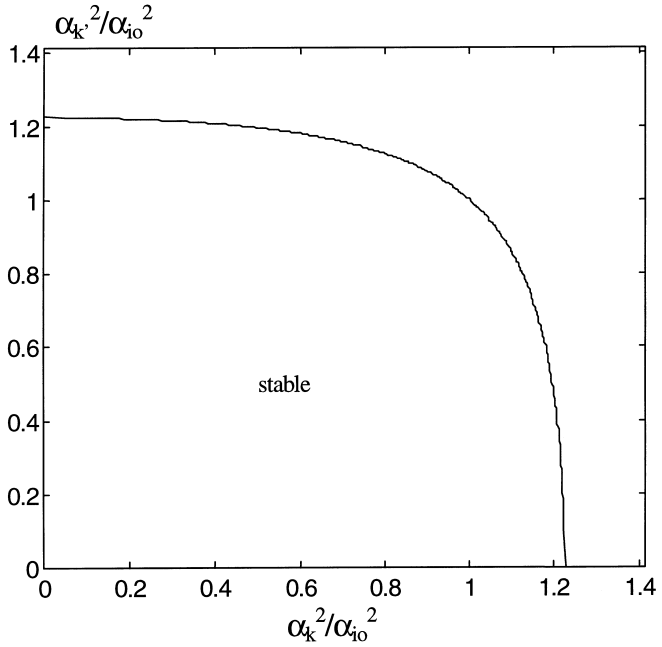

Fig. 16. Stability domain of a mode $i_0 = (p_0, q_0)$ of amplitude α_{i0} with respect to a perturbation $k = (p, q)$. It is plotted as a function of $\alpha_\kappa^2/\alpha_{i0}^2$ and $\alpha_{k'}^2/\alpha_{i0}^2$ where α_k and $\alpha_{k'}$ are the amplitudes at the limit cycle (given by Eqs. (8a)–(8c)) of the modes k and k' so that $k' = (2p_0 - p, 2q_0 - q)$.

(acoustic, optical, band) described above, or when modes with the same wavenumbers (but different frequencies) are considered then $\alpha_k = \alpha_{k'}$ and only the first diagonal in Fig. 16 is relevant. The roots are $\lambda = \alpha_k^2 - 2\alpha_{i0}^2 \pm \alpha_{i0}^2$ so that the stability criterion is just $\alpha_{i0}^2 > \alpha_k^2$, i.e. to be stable a mode must have the largest amplitude. According to these computations one should expect that the selected mode is the one with the largest amplitude. Note that the band mode should never be stable since two modes exist with similar amplitude.

References

[1] F. Giorgiutti, L. Laurent, F. Daviaud, Phys. Rev. E 58 (1) (1998).
[2] S. Houard, F. Daviaud, P. Bergé, Physica D 99 (1997), 318.
[3] G.B. Ermentrout, Physica D 41 (1990) 219–231.
[4] C. Matthews, R.E. Mirollo, S.H. Strogatz, Physica D 52 (1991) 293–331.
[5] V. Hakim, W.-J. Rappel, Phys. Rev. A 46 (12) (1992) 7347–7350.
[6] N. Nakagawa, Y. Kuramoto, Progr. Theoret. Phys. 89 (2) (1993) 313–323.
[7] E. Villermaux, E.J. Hopfinger, J. Fluid Mech. 263 (1994) 63–92.
[8] I. Peschard, P. Le Gal, Phys. Rev. Lett. 77 (15) (1996) 3122–3125.
[9] E. Villermaux, Phys. Rev. Lett. 75 (75) (1995) 4618–4621.
[10] H. Willaime, O. Cardoso, P. Tabeling, Phys. Rev. Lett. 67 (23) (1991) 3247.
[11] S. Houard, F. Daviaud, P. Bergè, Europhysics. Lett. 32 (2) (1995) 101–106.